Experimental verification of a theory for the time-resolved fluorescence spectroscopy of thick tissues

Albert E. Cerussi, John S. Maier, Sergio Fantini, Maria Angela Franceschini, William W. Mantulin, and Enrico Gratton

Fluorescence spectroscopy provides potential contrast enhancement for near-infrared tissue imaging and physiologically correlated spectroscopy. We present a fluorescence photon migration model and test its quantitative predictive capabilities with a frequency-domain measurement that involves a homogeneous multiple-scattering tissue phantom (with optical properties similar to those of tissue in the near infrared) that contains a fluorophore (rhodamine B). After demonstrating the validity of the model, we explore its ability to recover the fluorophore's spectral properties from within the multiple-scattering medium. The absolute quantum yield and the lifetime of the fluorophore are measured to within a few percent of the values measured independently in the absence of scattering. Both measurements are accomplished without the use of reference fluorophores. In addition, the model accurately predicts the fluorescence emission spectrum in the scattering medium. Implications of these absolute measurements of lifetime, quantum yield, concentration, and emission spectrum from within multiple-scattering media are discussed.

Key words: Fluorescence spectroscopy, photon migration, frequency domain, multiple scattering, tissue spectroscopy, diffusion theory, lifetime sensing, quantum yield.

1. Introduction

A. Advantages of Noninvasive Fluorescence in Tissues

Near-infrared (NIR) tissue spectroscopy and imaging offer many promising noninvasive medical applications such as the localization of tumors and the monitoring of physiological parameters such as hemoglobin saturation and glucose concentration.[1] Although NIR spectroscopy has been used successfully to measure hemoglobin saturation in tissues,[2] the detection of physiologically relevant compounds other than hemoglobin is more difficult (for example, the detection of glucose[3,4]). Traditionally, both the high sensitivity and the selectivity of fluorescence spectroscopy have made it an attractive tool for detecting traces of specific chemical compounds. Fluorescence offers enhanced sensitivity to NIR spectroscopy and enhanced image contrast.

There are many applications of *in vivo* fluorescence that are suitable for medical purposes. One example is safe, noninvasive, and inexpensive methods for tumor localization and treatment; certain fluorophores, such as a hematoporphyrin derivative, naturally concentrate inside tumor tissue when administered intravenously.[5] Selective tissue targeting is also possible with fluorophores engineered to bind to a specific target or with specific tissue markers such as antibodies. Other examples of fluorescence seek to supply medicine with noninvasive monitors of physiological processes. Phosphorescent quenching has been used to study local oxygen pressure in biological tissues.[6] In addition to fluorescence intensity, other fluorescence parameters such as the lifetime may also provide useful physiological information.[7] Fluorophores are currently available that exhibit measurable lifetime changes, depending on variations in parameters such as local pH.[8]

B. Noninvasive Fluorescence: The Problem of Multiple Scattering

For some time, fluorescence has been studied in highly scattering layers.[9,10] Light transport in tis-

The authors are with the Department of Physics, Laboratory for Fluorescence Dynamics, University of Illinois at Urbana-Champaign, 1110 W. Green Street, Urbana, Illinois 61801.

Received 16 April 1996; revised manuscript received 29 July 1996.

0003-6935/97/010116-09$10.00/0

sues is dominated by scattering processes within the visible and NIR regions of the spectrum.[11] Multiple scattering leads to a phenomenon called photon migration, in which individual photons can be thought of as undergoing a random walk through the tissue, traveling along a wide variety of complex paths. The general problem of multiple scattering of light inside tissuelike materials has received considerable attention in recent years.[12–14] Photon migration provides a foundation onto which we can build a quantitative model for fluorescence in strongly scattering media such as tissues. Knowledge of the spatial distribution of light inside a tissue is essential in order to take full advantage of noninvasive fluorescence.

The problem of fluorescence spectroscopy in scattering media has been investigated by the use of various scattering models.[15] Fluorescence emission spectra have already been recovered from thin tissue samples and have provided many promising diagnostic capabilities.[16] Quantitative models of the emission spectra in these tissue samples already exist.[17] The theory of fluorescence photon migration, which is suitable for thick tissues, has been addressed in both steady-state[18] and time-resolved cases.[19,20] Experiments in thick tissuelike materials, specifically those of a quantitative nature, have not yet been performed. Patterson and Pogue[19] have demonstrated that the fluorescence photon migration theory qualitatively describes experimental results. The basic method discussed by Patterson and Pogue has been extended by Li *et al.*[20] to include fluorescent inhomogeneities. In this paper we show that the model presented by Patterson and Pogue may be used to predict the values of absolute fluorescence parameters, such as intensity and phase. This approach allows accurate measurements of the fluorescence emission spectrum, the lifetime, the quantum yield, and the concentration of the fluorophore embedded within a multiple-scattering medium without the use of reference fluorophores.

2. Theory

A. Diffusion Theory

The diffusion equation is the standard approximation used to describe light transport inside strongly scattering media such as biological tissues[12–14,21]:

$$\frac{\partial U(\mathbf{r}, t)}{\partial t} - \nu D \nabla^2 U(\mathbf{r}, t) + \nu \mu_a U(\mathbf{r}, t) = q(\mathbf{r}, t), \quad (1)$$

where $\nu D = \nu(3\mu_s')^{-1}$ is the diffusion coefficient (in square centimeters per second), $q(\mathbf{r}, t)$ is the source term (in photons per cubic centimeter per second), and $U(\mathbf{r}, t)$ is the photon density (in photons per cubic centimeter) at position $\mathbf{r}$ (in centimeters) and time t (in seconds). In Eq. (1) we assume that all photons travel at one speed ν, which we take to be the speed of light in water. Equation (1) is valid for a macroscopically homogeneous medium. The diffusion equation relates the measurable photon density to the optical properties of the medium, namely the absorption coefficient μ_a (in inverse centimeters) and the reduced scattering coefficient μ_s' (in inverse centimeters). The inverse of μ_s' represents the mean free path between effectively isotropic scattering events,[22] whereas the inverse of μ_a represents the mean path length before absorption. We assume that these optical coefficients provide an adequate characterization of the medium.

In the frequency-domain approach, we implement a sinusoidally intensity-modulated point source,[12] modulated at angular frequency ω, to model the excitation light injected into the sample. Such a source has the form $q(\mathbf{r}, \omega, t) = P(\omega)\delta(\mathbf{r})\exp(-i\omega t)$, where $P(\omega)$ is the source strength (in photons per second) and $\delta(\mathbf{r})$ is the Dirac delta function. In the infinite medium geometry, the solution to Eq. (1) when this source is used yields the photon density $U(r, \omega)\exp(-i\omega t)$, where[12,23]

$$U(r, \omega) = \frac{P(\omega)}{4\pi\nu D}\frac{1}{r}\exp[-k(\omega)r], \quad (2)$$

$$k^2(\omega) \equiv \frac{\mu_a}{D}\left(1 - \frac{i\omega}{\nu\mu_a}\right). \quad (3)$$

Solutions to the diffusion equation in the frequency domain take the form of spherical photon density waves, where ik defines a complex wave vector, which is in units of inverse centimeters. The physics of these waves has been described elsewhere.[12,23–25]

B. Adding Fluorescence

Equation (1) can also be used to describe the propagation of fluorescence light inside a multiple-scattering medium, provided that we properly model the effective fluorescence source. To avoid confusion, coefficients at the excitation wavelength (λ_x) are denoted by the subscript x, and coefficients at the emission wavelength (λ_m) are denoted by the subscript m. Suppose that we distribute a fluorophore uniformly throughout a homogeneous multiple-scattering medium. This fluorophore creates an additional absorption μ_{afx} of the excitation light, where μ_{afx} is directly proportional to the fluorophore concentration through the molar extinction coefficient. With regard to the fluorophore, we make the following assumptions: (1) The fluorophore concentrations are dilute such that the probability that a fluorophore will absorb emission light and refluoresce (i.e., secondary fluorescence) is negligible, (2) the intensity decay occurs at a single rate (i.e., a single exponential decay profile), and (3) the photobleaching is negligible.

The emission source term $q_m(r, t)$ must be proportional to the excitation photon density at r and at t [i.e., $U_x(r, t)$] and also must be proportional to the fluorophore quantum yield (Λ). In the linear regime, the probability per unit time for the absorption of an excitation photon is given by $\nu\mu_{afx}$. Thus the strength of the emission scales with $(\nu\mu_{afx})\Lambda U_x(r, t)$. The fluorescence signal strength at λ_m is also deter-

mined by the emission spectrum of the fluorophore. The emission spectral efficiency may be expressed as a probability density $\varphi_m(\lambda)$, which is defined such that $\Lambda\varphi_m(\lambda)d\lambda$ gives the probability that after the absorption of a photon the fluorophore will radiate into a wavelength range $d\lambda$ about λ. The probability density $\varphi_m(\lambda)$ is also normalized to unity:

$$\int_0^\infty \varphi_m(\lambda)d\lambda = 1.$$

The lifetime τ (in nanoseconds) of the fluorophore induces a temporal delay of the fluorescence emission. This delay translates into a convolution between the distribution of decay times and the actual time at which the excitation photon is absorbed. The emission photon source then takes the form

$$dq_m(r, t) = \nu\mu_{afx}\left[\int_0^\infty U_x(r, t - t')\exp\left(-\frac{t'}{\tau}\right)\frac{dt'}{\tau}\right] \times \Lambda\varphi_m(\lambda_m)d\lambda_m, \quad (4)$$

where t' is the time of absorption by the fluorophore. In the frequency domain, the time dependence is given by $\exp(-i\omega t)$, so that the source term becomes $dq_m(r, \omega)\exp(-i\omega t)$, where

$$dq_m(r, \omega) = \Lambda\nu\mu_{afx}\left(\frac{1 + i\omega\tau}{1 + \omega^2\tau^2}\right)U_x(r, \omega)\varphi_m(\lambda_m)d\lambda_m. \quad (5)$$

Finally, we can determine the emission photon density by spatially convolving the Green's function at the emission wavelength [i.e., Eq. (2)] with the source term of Eq. (5). This convolution reflects the fact that excited fluorophores inside the sample at many positions contribute to the total emission photon density. The measured emission photon density becomes

$$U_m(r, \omega) = \frac{\Lambda\mu_{afx}\Phi_m P(\omega)}{4\pi\nu D_m D_x}\left(\frac{1 + i\omega\tau}{1 + \omega^2\tau^2}\right) \times \frac{1}{r}\frac{\exp[-k_x(\omega)r] - \exp[-k_m(\omega)r]}{[k_m^2(\omega) - k_x^2(\omega)]} \quad (6)$$

after all wavelength contributions passed by the nonideal detector are summed. The factor Φ_m, which contains the system spectral response as well as the fluorophore spectral emission efficiency, gives the detection efficiency of the system at λ_m and is described below in this paper. The results of this basic formalism agree with previous work.[19,20]

C. Analysis of the Fluorescence Photon Density

The emission photon density given by Eq. (6) is a convolution between emission and excitation photon density waves, so that the phases associated with emission and excitation photon migration do not add linearly. The amplitude of $U_m(r, \omega)$ gives the ac intensity [$U_m(r, 0)$ is the dc intensity], whereas the argument of $U_m(r, \omega)$ gives the phase of the emission photon density wave with respect to the phase of the excitation source. Equation (6) may be used to calculate the measured fluorescence at a given location, but it does not take into account secondary fluorescence emission (as mentioned in the assumptions above).

Equation (6) segments into three natural factors: a spatial factor that contains all of the spatial information (i.e., r dependence), a lifetime factor that contains all appearances of τ, and a fluorophore factor that contains the only appearance of Λ and is also proportional to μ_{afx}. Note that μ_{afx} also appears inside the k_x's. Only when $\mu_{afx} \ll \mu_{ax}$ is $U_m(r, t)$ strictly linear in fluorophore concentration.

3. Experimental Methods

A. Outline

Our experiment was designed to test Eq. (6) as a valid quantitative model for the propagation of fluorescence inside multiple-scattering media. A comparison was made between our measurements and the predictions of Eq. (6) for both the dc fluorescence intensity and the phase shift of the fluorescence as functions of r. Because the comparison required knowledge of the optical parameters of the fluorescent multiple-scattering medium, μ_{am}, μ'_{sm}, μ_{ax}, μ'_{sx}, μ_{afx}, Λ, and τ had to be measured independently. After confirming the validity of Eq. (6), we tested the model's ability to recover (1) the fluorophore quantum yield and concentration, (2) the fluorophore lifetime, and (3) the fluorescence emission spectrum.

B. Instrument

Figure 1 presents an outline of the major components used in our experiment. A mode-locked Nd:YAG laser pulsed at 76.2 MHz was frequency doubled to 532 nm to provide the excitation. (During the characterization of the phantom this Nd:YAG beam was used instead to pump a rhodamine 6G dye laser. See Subsection 3.D for details.) Laser output was then directed into a bifurcated fiber, where the main branch carried the light into the phantom. The minor branch of this fiber carried light to a reference detector to correct for laser fluctuations. A motorized scanner positioned the main branch of the fiber anywhere inside the phantom.

A separate detector optical fiber guided the light collected inside the phantom to an automated 8-nm FWHM bandwidth monochromator. After the monochromator, the light signal was carried by another fiber-optic cable to a heterodyned photomultiplier tube (PMT) for down-conversion of the high-frequency (76.2-MHz) signal. After digitization and Fourier transformation, this signal provided the frequency-domain information, namely the dc intensity, the ac amplitude, and the phase shift of the photon density wave.[26] The laser, synthesizers, and computer acquisition card were all phase locked.

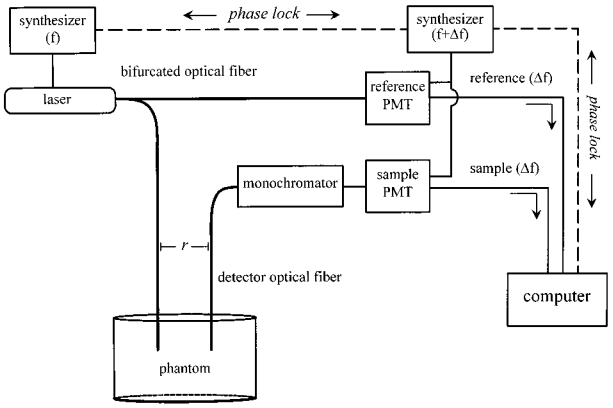

Fig. 1. Experimental apparatus. The dashed lines represent the locked phases between components, and the labeled frequencies give the signal frequency at each step (Δf is the beat frequency of 400 Hz). A frequency-doubled Nd:YAG laser pulsed at 76.2 MHz delivered light to the phantom by a fiber-optic cable (during the characterization of the phantom, this beam pumped a rhodamine 6G dye laser instead). A bifurcated optical fiber split the light such that most of the light excited the phantom and some of it acted as a reference. A detector fiber gathered light from the medium, and a monochromator then selected a particular wavelength bandpass. After heterodyning, a computer digitized the signal and then performed a Fourier transform. The positioning device for the detector fiber is not drawn for the sake of clarity. PMT's, photomultiplier tubes.

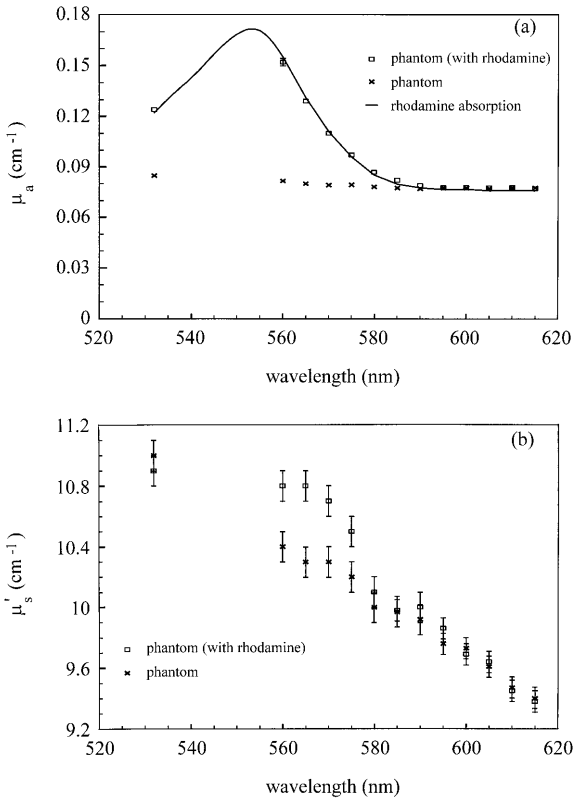

Fig. 2. Absorption and reduced scattering spectra. In both panels, the $\times$'s are the optical coefficients of the phantom without rhodamine B, and the open squares represent the optical coefficients of the same phantom mixed with rhodamine B. Panel (a) is a plot of the absorption coefficient versus wavelength. The solid curve is a rhodamine B spectrum measured independently without any scattering; however, for purposes of comparison, the phantom absorption (without rhodamine) has been added to this nonscattering spectrum. Thus this curve represents the absorption spectrum that we should observe for the rhodamine B inside the phantom. We can cleanly extract the fluorophore's absorption from the phantom. Panel (b) presents the reduced scattering coefficient versus wavelength. Rhodamine contributes little to the scattering. The precision uncertainty in the measurement of each coefficient is approximately 3%.

C. Phantom

Our tissue-simulating phantom consisted of an aqueous suspension of titanium dioxide particles (a scatterer) mixed together with black India ink (an absorber). The optical properties of this phantom were similar to those of tissue in the NIR ($\mu_a \sim 0.08$ cm^{-1}, $\mu_s' \sim 11$ cm^{-1}). We continuously mixed the medium at a location far from the optical fibers and also periodically stirred the solution by hand to prevent the settling of the titanium dioxide particles. The phantom was then made fluorescent by the addition of laser-grade rhodamine B to a final concentration of 380 nM. Rhodamine B in water decays as a single exponential[27] and is difficult to photobleach, and thus it satisfies two of the assumptions made about the fluorophore that were listed above. In a nonscattering medium, the lifetime of rhodamine B in water ($\tau = 1.50 \pm 0.01$ ns) was measured with a phase and modulation fluorometer, and we used a published value for the quantum yield ($\Lambda = 0.31$).[27] We assumed that these fluorescence parameters were unaffected by the titanium dioxide suspension.

D. Characterization of the Phantom

As stated above, the absorption and the reduced scattering coefficients of the phantom at the excitation and the emission wavelengths must be measured independently. For several wavelengths within the rhodamine B emission spectrum, we measured the optical coefficients of the phantom both with and without the fluorophore. The measurement protocol involved using a single modulation frequency (76.2 MHz) for the excitation source and scanning the detector fiber to collect light at multiple source–detector separations.[28] For this characterization of the optical properties of the phantom, we excited and detected light at the same wavelength and therefore did not measure any appreciable fluorescence. A tunable dye laser pumped by the Nd:YAG provided the wavelengths between 560 and 620 nm.

Without rhodamine, the phantom possessed absorption coefficients ranging between 0.078 and 0.084 cm^{-1} [Fig. 2(a)] and reduced scattering coefficients ranging between 9.3 to 11.0 cm^{-1} [Fig. 2(b)], depending on the wavelength. In both plots, the squares and the $\times$'s represent the phantom's optical coefficients measured with and without rhodamine, respectively. The curve in Fig. 2(a) is the absorption spectrum of rhodamine B in water at a concentration of 380 nM, measured independently in a spectrophotometer (i.e., without any scattering). Overall, Fig.

2 demonstrates the effects of the rhodamine B on the phantom's absorption and reduced scattering coefficients. Diffusion theory, which is the basis for our multidistance measurement protocol, allowed us to separate the effects of absorption and scattering effectively. In other words, we extracted the rhodamine B absorption spectrum from within a strongly scattering phantom as demonstrated by Fantini *et al.*[28] Our instrument's 0.1° phase error and less than 1% count error led to an uncertainty in precision of ~3% in each optical coefficient.

E. Fluorescence of the Phantom

The principal step of the experiment involved measuring the fluorescence of the rhodamine B from within the phantom. Here we excited the phantom with the Nd:YAG laser and monitored the fluorescence by setting the monochromator to the desired emission wavelength λ_m. In this step, we again performed a series of multidistance measurements over a few centimeters of source–detector separations by fixing λ_x at 532 nm and varying λ_m from 560 to 620 nm in 5-nm steps. The phantom without rhodamine does not fluoresce appreciably.

F. Calibration and Φ_m

There are two calibrations that we performed in order to measure absolute values of dc counts and phase. (Note that absolute dc intensity refers to an arbitrary number of counts. We neither counted photons nor measured the actual collected intensity, but instead measured a quantity that is proportional to the photon flux at the detector.) The first calibration involved determining the source strength $P(\omega)$ and the source phase. Knowledge of the source strength allowed us to translate equivalent source photon intensities into PMT counts, and the source phase is simply an offset. Measurements of both dc and phase at 532 nm at a known distance r allowed the calculation of the source terms by means of Eq. (2). The laser was not adjusted after this calibration.

Second, we also carefully characterized our detection system. The PMT and the monochromator taken together have a spectral intensity response denoted by $\gamma(\lambda)$. We determined this function by measuring the dc emission spectrum collected from quinine sulfate dihydrate, as quinine sulfate dihydrate has a well-characterized fluorescence spectrum.[29] Thus we corrected for the system's nonuniform spectral response.

Once $\gamma(\lambda)$ was known, we were then able to calculate Φ_m. The monochromator has a finite bandwidth that passes a range of wavelengths $\Delta\lambda$ centered about λ_m. Adding up all of the contributions to the measured signal within the detector bandpass, we find the expression for the factor Φ_m:

$$\Phi_m \equiv \int_{\lambda_m-\frac{\Delta\lambda}{2}}^{\lambda_m+\frac{\Delta\lambda}{2}} \varphi_m(\lambda_m')\gamma(\lambda_m')\mathrm{d}\lambda_m'. \qquad (7)$$

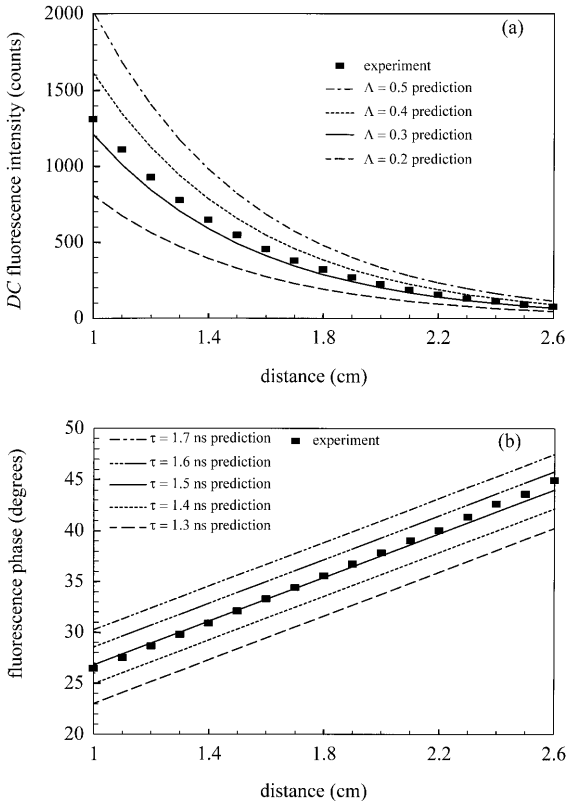

Fig. 3. Fluorescence versus source–detector separation at 580 nm. In both plots, the filled squares are the measured values and the curves are the predictions of the theory. There are no fitting parameters of any kind in this plot; however, the predictions are based on independent measurements of the optical coefficients. Panel (a) is a plot of the dc fluorescence intensity as a function of distance. The four curves are four predictions of the dc fluorescence intensity for Λ values of 0.2, 0.3, 0.4, and 0.5. Note that these predictions are independent of τ. The average value of Λ needed to make the measurement at a given r coincide with its prediction is 0.34 ± 0.01 for all the sampled r's, which agrees well with the published value of 0.31. Panel (b) is a plot of the phase of the fluorescence as a function of distance. The five curves are five predictions of the phase for τ values of 1.3, 1.4, 1.5, 1.6, and 1.7 ns. Note that these predictions are independent of Λ. The average value of τ needed to make the measurement at a given r coincide with its prediction for all the sampled r's is 1.52 ± 0.02 ns, which agrees well with the independently measured value of 1.50 ± 0.01 ns. The experimental measurement errors are 0.1° for phase and less than 1% for dc counts.

Numerical evaluation of this integral allows quantitative predictions of the detected signal measured at λ_m. In Eq. (7), $\varphi_m(\lambda)$ is the properly normalized emission spectrum of rhodamine B in water after the measured emission spectrum is deconvolved in water and the monchromator bandpass is taken into account (see Subsection 2.B).

4. Experimental Results

Given the measured absorption and reduced scattering coefficients as well as τ and Λ, the fluorescence photon migration model given by Eq. (6) accurately predicted the measured fluorescence photon density wave over the sampled wavelength region. Figure 3

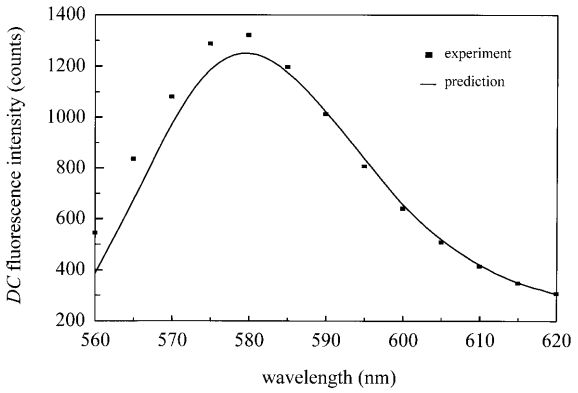

Fig. 4. dc fluorescence emission spectrum. The filled squares represent the measured dc fluorescence intensity at each wavelength for a fixed source–detector separation of 1 cm. The curve is again the prediction of Eq. (6) for each wavelength, also at a 1-cm source–detector separation. The agreement is excellent in the red part of the emission spectrum. There is less than a 10% discrepancy between the curves for the wavelengths ranging from 570 to 580 nm.

presents the measured frequency-domain fluorescence parameters (taken at 580 nm) plotted against their corresponding predictions from Eq. (6). The measured fluorescence quantities are represented by the filled squares, and the predictions are represented by the curves in both panels of Fig. 3. Recall that these predictions are based on the independently measured optical coefficients of the phantom.

The dc fluorescence intensity is plotted as a function of source–detector separation in Fig. 3(a). The four curves are predictions of Eq. (6) with four different values of the rhodamine B quantum yield. There are no fitting parameters involved in this plot; the intensities are absolute predictions (that is, after the source strength calibration). If we determine the value of Λ needed to make the prediction coincide with the measurement at a given r, we obtain a value of $\Lambda = 0.34 \pm 0.01$ as the average over all the sampled r's. This value is in good agreement with the published value of 0.31.

Similarly, we show the predictions of the phase of Eq. (6) plotted against the measured data in Fig. 3(b). Once again, there are no fitting parameters involved with the predictions, but this time the predictions for five different values of the rhodamine B lifetime are shown. We obtained an average value of $\tau = 1.52 \pm 0.02$ ns by calculating the value of τ needed to make the prediction coincide with the measured value for each of the sampled r's. This is in excellent agreement with the independently measured value of 1.50 ± 0.01 ns obtained from a measurement with a frequency-domain fluorometer of rhodamine B in water.

The measured and predicted dc fluorescence spectrum of rhodamine B in the scattering medium at a source–detector separation of 1 cm is shown in Fig. 4, in which the measured spectrum is the average of two different data sets, and the prediction has been interpolated to fill in missing values between the 5-nm sampling points. Over the range where the rhodamine absorbs poorly ($\lambda > 575$ nm), the agreement is excellent between prediction and experiment. Once again, this prediction is not a fit. The agreement grows poorer as we move toward the absorption maximum of rhodamine B (~555 nm).

5. Discussion of Results

A. Lifetime Determination

The fluorescence photon migration model accurately distinguishes between changes in the fluorescence phase shift emerging from photon migration and from the fluorophore lifetime. This was especially important in this experiment, as the photon migration times were comparable with τ. Another important feature of the model is that although both τ and Λ may be parameters that are sensitive to a given fluorophore's local environment, τ was obtained without knowledge of Λ, as the dc intensity is insensitive to τ and the phase shift is insensitive to Λ.

The values of τ obtained for all wavelengths agreed within 0.02 ns of each other; an important fact is that this was done without the use of a reference fluorophore. As previously described in the literature, lifetime determinations with[30] and without[31] the use of a reference fluorophore have already been undertaken. Accurate lifetime measurement is a major step toward the realization of lifetime sensing in tissues. However, our work does not address the more physiologically realistic complication of adding background fluorescence with a different lifetime.

B. Fluorescence Spectra

Multiple scattering also greatly complicates efforts to obtain emission spectra from tissuelike materials.[32] The fluorescence photon migration model was able to predict the changes to a nonscattering emission spectrum that were due to the absorption and the scattering of the medium. One cannot help but note that the discrepancy between prediction and experiment increases as the absorption of the fluorophore increases. Although the fluorophore concentration was below the micromolar range, the photon path length was ~30 cm in the medium, leading to some potential reabsorption of fluorescence light. This absorption effect is taken into account by the model because we have inserted the absorption coefficient of the medium with rhodamine present at the emission wavelength into Eq. (6). However, the discrepancy observed in Fig. 4 is unlikely the result of secondary fluorescence. In fact, reemission processes should affect the phase significantly, whereas the predicted phases agree with the measured phases within a few tenths of a degree.

At this time, we believe the reason for the discrepancy of Fig. 4 was due to a systematic error in the determination of the optical coefficients, as described in Subsection 3.D. For example, note in Fig. 2(b) that the scattering appears to change by the addition of rhodamine. The separation of scattering and absorption may have been corrupted, even if only mar-

ginally. We also point out that the prediction can be made to agree with the experiment within the experimental uncertainties of the measured optical coefficients.

A more rigorous approach involves fitting Eq. (6) to the measured data, thus eliminating the need to characterize the medium over the emission spectrum. The emission absorption and scattering coefficients of the medium can, in principle, be determined by a fit with knowledge of only the spatial dependence of the fluorescence emission. We had previously developed an instrument that performs a multidistance frequency-domain measurement on a semi-infinite medium in less than a second.[33] Because we can easily characterize a medium at the excitation wavelength with a multidistance measurement, the fit could eliminate the need for a light source at each emission wavelength in order to find the medium's optical coefficients over the emission spectrum (as we did in this experiment).

C. Concentration and Quantum Yield Determination

The most exciting aspect of absolute dc intensity measurements is that we now may use the fluorescence photon migration model to determine the product of $\Lambda\mu_{afx}$. The concentration and the quantum yield of the fluorophore are essentially restricted within the prefactor of Eq. (6). Therefore the dc intensity can be used to measure absolute quantum yields in systems in which the concentration of the fluorophore is known. Reciprocally, for a fluorophore in systems with a known Λ, one can retrieve the concentration of a uniformly distributed fluorophore in a multiple-scattering medium. Medical applications demand the ability to detect variations in fluorophore concentration, a problem that has been addressed by Li *et al.*[20]

An important point is that we were able to obtain the absolute quantum yield value without the use of a reference compound. Traditionally, absolute measurements of Λ have been difficult to perform in fluorescence spectroscopy. Current methods are hampered because of unavoidable geometric factors brought on by the differences between excitation and emission light paths.[34] In the turbid medium, the excitation and emission signals are detected with the same detector in the same geometry, which eliminates the necessity of accounting for the geometric effects through empirical factors.

D. Sensitivity to Fluorophore Concentration

Fluorescence spectroscopy is typically more sensitive than absorption spectroscopy in the detection of small fluorophore concentrations because of the improved signal-to-noise ratio (SNR). Figure 5 presents a theoretical comparison between fluorescence and differential absorption methods (based on changes in the signal before and after the addition of the fluorophore). This comparison uses the medium parameters measured at 580 nm (which are given in Table 1), with a modulation frequency of 76.2 MHz and a source–detector separation of 2 cm. The plot compares the emission dc intensity (solid curve) with the excitation dc intensity (dashed curve) as functions of rhodamine B concentration. The slopes of these lines determine the sensitivity to the fluorophore concentration. The inset of Fig. 5 is a plot of the fractional change between the dc intensity at concentration x and the dc intensity at concentration $x + 10$ nM. This fractional change is then divided by the uncertainty of the measurement, which is of the order of 0.4% in terms of counts. The fluorescence intensity provides superior sensitivity for small concentrations, but loses its sensitivity advantage over differential absorption after ~350 nM (which is 0.036 cm^{-1} in absorption). The sensitivity of the dc intensity will change with the source–detector separation for both fluorescence and differential absorption.[19] Fluorescence is superior to differential absorption over a larger range of concentrations as the source–

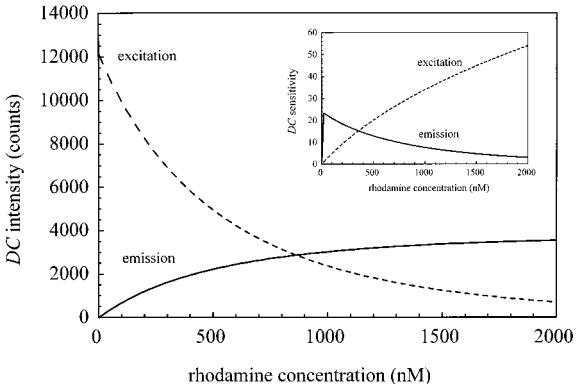

Fig. 5. Theoretical dc sensitivity comparison. Values for the plots are found in Table 1. The modulation frequency was 76.2 MHz and the source–detector separation was $r = 2$ cm. The solid curve represents the fluorescence dc intensity calculated from the emission photon density [Eq. (6)], and the dashed curve represents the excitation dc intensity calculated from the excitation photon density [Eq. (2)]. The inset graph is the dc sensitivity, which is defined as the fractional change in counts with a 10-nM change in concentration (see the text for the definition). The fluorescence dc sensitivity SNR is superior to the excitation absorption dc sensitivity SNR for small fluorophore concentrations, but after ~350 nM the fluorescence begins to saturate, and hence loses sensitivity. This crossing-over point of the sensitivities depends on the source–detector separation.

Table 1. Medium Parameters for Theoretical Sensitivity Plots[a]

Parameter	λ_x (532 nm)	λ_m (580 nm)
Reduced scattering coefficient (cm^{-1})	$\mu'_{sx} = 10.9$	$\mu'_{sm} = 10.1$
Background absorption coefficient (cm^{-1})	$\mu_{ax} = 0.0849$	$\mu_{am} = 0.0782$
Fluorophore molar extinction coefficient ($M^{-1} \times cm^{-1}$) ($\times 10^4$)	4.52	1.16

[a]These are the values for the optical coefficients used for the plots in Figs. 5 and 6 that were determined from our multidistance measurement on the phantom with rhodamine B. The fluorophore molar extinction coefficients were measured in a standard spectrophotometer and were taken to base 10.

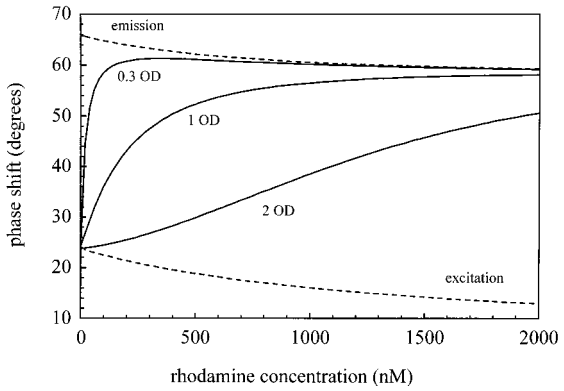

Fig. 6. Theoretical phase-sensitivity comparison. The lower dashed curve represents the phase versus concentration as predicted by the excitation photon density [Eq. (2)], and the upper dashed curve represents the same thing, but predicted by the fluorescence photon density [Eq. (6)]. All variables are the same as those used in Fig. 5. Note that except for the lifetime effect, the curves are quite similar and are not useful for determining the fluorophore concentration. However, a phasor combination of both signals results in a vastly improved phase sensitivity with respect to fluorophore concentration. The amount of attenuation of the excitation relative to the emission is listed in the figure for optical densities of 0.3, 1, and 2.

detector separation decreases. For example, the largest concentration at which the fluorescence SNR exceeds the differential absorption SNR changes from about 780 to 200 nM as the source–detector separation changes from 1 to 3 cm, respectively.

The phase sensitivity is essentially the same for the fluorescence signal as it is for the differential absorption signal. This comes as no surprise, as a distinctive advantage of phase measurements in fluorescence is its insensitivity to intensity (and hence to fluorophore concentration). Figure 6 demonstrates this effect. The lowest dashed curve represents the phase as a function of rhodamine B concentration for the excitation photon density wave alone, calculated by the use of Eq. (2) with the excitation coefficients. The upper dashed curve represents the phase of the fluorescence, calculated with Eq. (6). All parameters are the same as those used in Fig. 5. Essentially the only difference between these curves is the initial phase shift that is due to the fluorophore lifetime. In either case, the change in phase over a 50-nM range is comparable with the detection limit of our system (0.1°).

However, we can take advantage of this fluorescence phase shift by combining both excitation and emission signals to enhance the overall sensitivity of the phase to the fluorophore concentration. (Note that this must be done with phasor addition). The remaining curves in Fig. (6) represent different combinations of the excitation and the emission photon densities, in which the excitation signal has been cut by 0.3, 1, and 2 optical-density units. The sensitivity of the phase to fluorophore concentration is now much improved, especially in the low-concentration regime.

6. Conclusion

In agreement with other groups, we have derived an expression to quantify fluorescence photon migration in thick tissues. Not only have we further verified the qualitative character of the equation, but we have also demonstrated its abilities for quantitative predictions of fluorescence parameters. This equation is accessible to a full range of applications for fluorescence spectroscopy in tissues, allowing the determination of fluorescence parameters such as concentrations, lifetimes, quantum yields, and emission spectra without the difficulty of reference compounds. By using a fit, we may be able to perform these measurements by using only one light source at the excitation wavelength. This would allow for much simpler implementation of fluorescence spectroscopy to multiple-scattering media.

Support for this work came from the U.S. National Institutes of Health grant CA57032, the U.S. National Institutes of Health grant RR03155 (LFD grant), and the University of Illinois. The authors also thank Todd French for his measurement of the lifetime of rhodamine B in water.

References

1. *Biomedical Optical Spectroscopy and Diagnostics*, D. Benaron and E. Sevick-Muraca, eds., 1996 OSA Technical Digest (Optical Society of America, Washington D.C., 1996); *Advances in Optical Imaging and Photon Migration*, R. Alfano and J. Fujimoto, eds., 1996 OSA Technical Digest, (Optical Society of America, Washington D.C., 1996).
2. R. A. De Blasi, S. Fantini, M. A. Franceschini, M. Ferrari, and E. Gratton, "Cerebral and muscle oxygen saturation measurement by frequency-domain near infra-red spectrometer," Med. Biol. Eng. Comput. **33,** 228–230 (1995).
3. J. S. Maier, S. A. Walker, S. Fantini, M. A. Franceschini, and E. Gratton, "Possible correlation between blood glucose concentration and the reduced scattering coefficient of tissues in the near infrared," Opt. Lett. **19,** 2062–2064 (1994).
4. M. Kohl, M. Cope, M. Essenpreis, and D. Böcker, "Influence of glucose concentration on light scattering in tissue-simulating phantoms," Opt. Lett. **19,** 2170–2172 (1994).
5. B. C. Wilson and M. S. Patterson, "The physics of photodynamic therapy," Phys. Med. Biol. **31,** 327–360 (1986).
6. W. L. Rumsey, J. M. Vanderkooi, and D. F. Wilson, "Imaging of phosphorescence: a novel method for measuring oxygen distribution in perfused tissue," Science **241,** 1649–1651 (1988).
7. H. Szmacinski and J. R. Lakowicz, "Lifetime-based sensing," in *Probe Design and Chemical Sensing*, J. R. Lakowicz, ed., Vol. 4 of Topics in Fluorescence Spectroscopy (Plenum, New York, 1994), pp. 295–334.
8. H. Szmacinski and J. R. Lakowicz, "Optical measurements of pH using fluorescence lifetimes and phase-modulation fluorometry," Anal. Chem. **65,** 1688–1674 (1993).
9. E. Allen, "Fluorescence white dyes: calculation of fluorescence from reflectivity values," J. Opt. Soc. Am. **54,** 506–515 (1964).
10. G. R. Seely, "Transport of fluorescence through highly scattering media: corrections to the determinations of quantum yields," Biophys. J. **52,** 311–316 (1987).
11. B. C. Wilson, M. S. Patterson, S. T. Flock, and D. R. Wyman, "Tissue optical properties in relation to light propagation models and *in vivo* dosimetry," in *Photon Migration in Tissues*, B. Chance, ed. (Plenum, New York, 1989), pp. 25–42.
12. J. B. Fishkin and E. Gratton, "Propagation of photon-density

waves in strongly scattering media containing an absorbing semi-infinite plane bounded by a straight edge," J. Opt. Soc. Am. A **10,** 127–140 (1993).
13. M. S. Patterson, B. Chance, and B. C. Wilson, "Time-resolved reflectance and transmittance for the non-invasive measurement of tissue optical properties," Appl. Opt. **28,** 2331–2336 (1989).
14. A. Ishimaru, *Wave Propagation and Scattering in Random Media* (Academic, New York, 1978).
15. D. Oelkrug, "Fluorescence spectroscopy in turbid media and tissues," in *Probe Design and Chemical Sensing*, J. R. Lakowicz, ed., Vol. 4 of Topics in Fluorescence Spectroscopy (Plenum, New York, 1994), pp. 223–253.
16. R. Richards-Kortum, R. P. Rava, M. Fitzmaurice, L. L. Tong, N. B. Ratliff, J. R. Kramer, and M. S. Feld, "A one layer model of laser-induced fluorescence for diagnosis of disease in human tissue: applications to atherosclerosis," IEEE Trans. Biomed. Eng. **36,** 1222–1232 (1989).
17. A. J. Durkin, S. Jaikumar, N. Ramanujam, and R. Richards-Kortum, "Relation between fluorescence of dilute and turbid samples," Appl. Opt. **33,** 414–423 (1994).
18. J. Wu, M. S. Feld, and R. P. Rava, "Analytical model for extracting intrinsic fluorescence in turbid media," Appl. Opt. **32,** 3585–3595 (1993).
19. M. S. Patterson and B. W. Pogue, "Mathematical model for time-resolved and frequency-domain fluorescence spectroscopy in biological tissues," Appl. Opt. **33,** 1963–1974 (1994).
20. X. D. Li, M. A. O'Leary, D. A. Boas, B. Chance, and A. G. Yodh, "Fluorescent diffuse photon density waves in homogeneous and heterogeneous turbid media: analytic solutions and applications," Appl. Opt. **35,** 3746–3758 (1996).
21. J. J. Duderstadt and L. J. Hamilton, *Nuclear Reactor Analysis* (Wiley, New York, 1976), pp. 133–145.
22. R. F. Bonner, R. Nossal, S. Havlin, and G. H. Weiss, "Model for photon migration in turbid biological media," J. Opt. Soc. Am. A **4,** 423–432 (1987).
23. S. R. Arridge, M. Cope, and D. T. Delpy, "Theoretical basis for the determination of optical path lengths in tissue: temporal and frequency analysis," Phys. Med. Biol. **37,** 1537–1560 (1992).
24. A. Yodh and B. Chance, "Imaging and spectroscopy using diffusing light," Phys. Today **48**(3), 34–40 (1995).
25. D. A. Boas, M. A. O'Leary, B. Chance, and A. G. Yodh, "Scattering and wavelength transduction of diffuse photon density waves," Phys. Rev. E **47,** 2999–3002 (1993).
26. B. Feddersen, D. W. Piston, and E. Gratton, "Digital parallel acquisition in frequency-domain fluorometry," Rev. Sci. Instrum. **60,** 2929–2936 (1989).
27. F. López Arbeloa, T. López Arbeloa, M. J. Tapia Estévez, and I. López Arbeloa, "Photophysics of rhodamines: molecular structure and solvent effects," J. Phys. Chem. **95,** 2203–2208 (1991).
28. S. Fantini, M. A. Franceschini, J. B. Fishkin, B. Barbieri, and E. Gratton, "Quantitative determination of the absorption spectra of chromophores in strongly scattering media: a light-emitting-diode based technique," Appl. Opt. **33,** 5204–5213 (1994).
29. R. A. Velapoldi and K. D. Mielenz, "A fluorescence standard reference material: quinine sulfate dihydrate," NBS Spec. Publ. 260-64 (National Bureau of Standards, U.S. Government Printing Office, Washington, 1980).
30. C. L. Hutchinson, J. R. Lakowicz, and E. M. Sevick-Muraca, "Fluorescence lifetime-based sensing in tissues: a computational study," Biophys. J. **68,** 1574–1582 (1995).
31. C. L. Hutchinson, T. L. Troy, and E. M. Sevick-Muraca, "Fluorescence-lifetime determination in tissues or other scattering media from measurement of excitation and emission kinetics," Appl. Opt. **35,** 2325–2332 (1996).
32. S. A. Ahmed, Z.-W. Zang, K. M. Yoo, M. A. Ali, and R. R. Alfano, "Effect of multiple light scattering and self-absorption on the fluorescence and excitation spectra of dyes in random media," Appl. Opt. **33,** 2746–2750 (1994).
33. S. Fantini, M. A. Franceschini-Fantini, J. S. Maier, S. A. Walker, B. Barbieri, and E. Gratton, "Frequency-domain multi-channel optical detector for non-invasive tissue spectroscopy and oximetry," Opt. Eng. **34,** 32–42 (1995).
34. J. N. Demas and G. A. Crosby, "The measurement of photoluminescence quantum yields: a review," J. Phys. Chem. **75,** 991–1024 (1971).